Conformation and dynamics of a tethered active polymer chain

Chao Wang [1,*] Yanli Zhou,[1] Xiao Yang,[1] Yingcai Chen,[1] Yifan Shen,[2] and Mengbo Luo[2,†]

[1]*Department of Physics, Taizhou University, Taizhou 318000, Zhejiang, China*
[2]*Department of Physics, Zhejiang University, Hangzhou 310027, Zhejiang, China*

The conformational and dynamical properties of a tethered semiflexible polymer chain under tangential active force (f_a) are studied by using the Langevin dynamics simulation method. The head of the polymer is fixed near an infinite flat surface at $z = 0$. The polymer is equilibrated first at $f_a = 0$ and then subjected to the active force. Under the influence of the active force, the polymer is gradually compressed. Specially, for large f_a and large bending rigidity (k_b), the polymer is buckled into a quasihelical structure rotating around the z axis at the steady state. It is found that both the radius of the quasihelical structure (R) and the angular velocity of the rotation (ω) are nearly independent of the polymer length (N), but show scaling relations with f_a and k_b, i.e., $R \propto f_a^{-1/3} k_b^{1/3}$ and $\omega \propto f_a^{4/3} k_b^{-1/3}$, which are explained by simple dynamical models. Before reaching the steady state, it is further found that the buckling velocity of the polymer is proportional to f_a but roughly independent of k_b and N, then the buckling time (t_b) can be described by a scaling relation $t_b \propto N f_a^{-1}$. The underlying mechanism of the buckling process is revealed.

I. INTRODUCTION

In recent years, the conformational and dynamical properties of the natural or artificial active polymers have been a topic with rapidly growing interest in the biological, the physical, and the chemical communities. One important example of active polymers is the microtubule which can exhibit activity under the driving force exerted by motor proteins and kinesin and dynein motors [1–6]. Another important example of active polymers is the linear chain formed by connecting active colloids [7,8]. The active polymer systems are inherently nonequilibrium, and their properties are important in biology and technological applications, such as DNA, RNA, and microtubules under the force of molecular motors [9], load transport by using self-propelled chains [10–12], and are also useful for understanding the collective phenomena and nonequilibrium statistical mechanics.

It was found that active polymers often show many interesting features, which are different from that of passive polymers. Ghosh and Gov studied the dynamics of semiflexible polymers with active force described by an exponentially correlated colored noise, and found that the polymer can show enhanced diffusion and spatial correlation of local displacements depending on the thermal mode, the elastic mode of the polymer, and the duration of the activity [13]. Osmanović and Rabin found that the dynamics of the Rouse polymer is dependent on the temporal and contour separation correlations of the active fluctuation noise [14]. When the temporal correlations are characterized by a single time scale, there is a transition from normal diffusion to superdiffusion at intermediate time

scales. While when multiple time scales are involved, there is a transition from subdiffusion to normal diffusion at times much shorter than the longest Rouse time of the polymer [14]. For self-avoiding polymers formed by active Brownian particles, it was found that the polymer initially shrinks and then swells with increasing the active force, and shows faster relaxation than the Rouse polymer at moderate active force [15–21].

Theoretically and simulationally, active polymer with tangential force is often adopted to study the conformation and the dynamics of microtubules or filaments driven by protein motors in gliding motility assays, in which the tails of the motor proteins are firmly attached on the substrate, while the heads of the proteins bind to the microtubules and exert forces along the contour of the microtubules. It was found that the conformation and the dynamics of the polymer often exhibit remarkable dependence on the strength of the active force. In two-dimensional (2D) system, active polymers can spontaneously form stable spirals at strong active force and small bending rigidity, and move along its own contour in a railway-motion manner at weak active force [22]. When the head of the active polymer is bound to a passive load, the polymer can push the load with different conformational states and motion types depending on the strength of the active force and the hydrodynamic friction of the load, meanwhile, the speed and the efficiency of load transport are dependent on the dynamical conformation of the polymer [23,24]. In three-dimensional (3D) system, linear flexible polymers were found to undergo a coil-to-globule transition, and the diffusion coefficient of the polymer becomes essentially independent of the polymer length for long polymers or large active force [25]. The conformation is also dependent on the topology and the rigidity of the polymer. Locatelli *et al.* found that ring polymers show an inflation-to-collapse transition with

*chaowang0606@126.com
†luomengbo@zju.edu.cn

increasing polymer length at large active force [26]. For semi-flexible polymers, the active force can decrease effectively the stiffness of the polymer, leading to the monotonic decrease of the polymer size with the active force [27]. Meanwhile, it was found that the motion of the polymer shows three distinct types, namely, translation, snaking, and rotation, depending on the polymer rigidity and the active force, and the diffusion coefficient grows linearly with a renormalized activity parameter [28,29]. Further studies indicated that the conformation and the dynamics of the polymer are also dependent on the orientation and the location of the active force along the polymer [15,30–33].

When the active polymer's head is fixed, its behavior is more complex than the free polymer. In 2D space, the polymer shows spiral form and rotational motion when the head is fixed by a frictionless pivot, and exhibits wave form and flapping motion when the head is pinned by a clamp [34–37]. Both the rotational frequency for the former and the flapping frequency for the latter show the same dependence on the strength of the active force and the bending rigidity of the polymer [34,37]. In 3D space, it was found that a nonthermal active polymer with the head being clamped shows two distinct oscillaroty modes, a nonplanar spining rotation at relatively small activity and a planar beating motion at large activity, which is more complex than that in 2D space [32,38].

Recent studies indicated that active polymers near spatial boundaries also show interesting properties. Xu *et al.* studied the dynamics of active polymers with chirality in a transversal asymmetric channel, and found that the transport direction of the polymer can be rectified and even show current reversals due to the competition of the chirality of the polymer and the properties of the channel [39]. Shen *et al.* studied the conformation and dynamics of active polymers on the surface of a cylinder, and found that there are three typical (spiral, helix-like, and rodlike) conformations and three specific (rotational, snakelike, and straight translational) motion types [40]. Motivated by this, we here study the conformational and dynamical properties of a semiflexible active polymer with the head fixed at an infinite surface. The polymer is equilibrated first and then subjected to a tangential active force along its contour. Specially, for large active force and large bending rigidity, the polymer chain is compressed and buckled into quasihelical structures with rotational motion at the steady state. Moreover, before reaching the final steady state, the polymer undergoes a buckling process, during which the monomers of the polymer are found to move in a railway-motion manner with a constant velocity.

II. SIMULATION MODEL AND METHOD

Simulations are carried out in the 3D space. Figure 1 shows a 2D sketch of the model system. In the space $z > 0$, there is a polymer chain with its head fixed near an infinite flat surface at $z = 0$. The surface is impenetrable for the polymer chain.

In our simulation, the polymer chain is mimicked by an off-lattice bead-spring chain model, where the chain is composed of sequentially connected monomers numbered from 1 to N. The total internal potential energy of a polymer chain includes the repulsive energy between monomers, the bond energy, and the bond bend energy. The repulsive en-
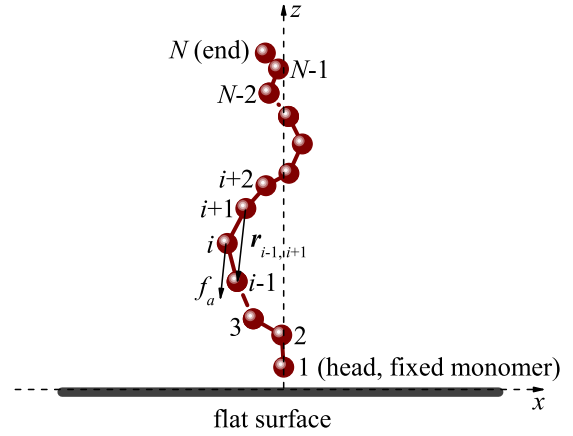
FIG. 1. A 2D sketch of the simulation model system. The head monomer of the polymer chain is tethered near the surface at $z = 0$. The ith monomer ($1 < i < N$) is subjected to a tangential force f_a along the vector $\boldsymbol{r}_{i-1,i+1}$ between the position of the monomers $i-1$ and $i + 1$.

ergy between monomers is described by the purely repulsive Weeks-Chandler-Andersen (WCA) potential,

$$U_{LJ}(r) = \begin{cases} 4\varepsilon_0\big[\big(\frac{\sigma}{r}\big)^{12} - \big(\frac{\sigma}{r}\big)^6\big] + \varepsilon_0, & r \leqslant 2^{1/6}\sigma \\ 0, & r > 2^{1/6}\sigma \end{cases}, \quad (1)$$

where r is the distance between two monomers, ε_0 is the interaction strength, σ is the diameter of monomers. The bond energy between bonded monomers is described by the finitely extensible nonlinear elastic (FENE) potential:

$$U_{\text{FENE}}(r) = -\frac{k}{2}R_0^2 \ln\left[1 - \left(\frac{r}{R_0}\right)^2\right], \quad (2)$$

where k is the spring constant, and r and R_0 represent the bond length and the maximum bond length, respectively. The bending energy between two adjacent bonds is described by

$$U_{\text{bend}} = k_b(\theta - \theta_0)^2. \quad (3)$$

Here θ is the angle between two neighboring bond vectors, and k_b is the bending rigidity. In our simulation we set $\theta_0 = 0$, i.e., $U_{\text{bend}} = 0$ when the two neighboring bonds are in a straight line.

The head monomer of the polymer chain is fixed at $(0, 0, \sigma)$. The interactions between other monomers (from 2 to N) and the surface at $z = 0$ are also described by the WCA potential [Eq. (1)], where r represents the nearest distance between monomers and the surface.

To model the active polymer chain, we assume that the ith monomer ($1 < i < N$) is acted on by a tangential force,

$$\boldsymbol{F}_a^{(i)} = f_a \frac{\boldsymbol{r}_{i-1,i+1}}{|\boldsymbol{r}_{i-1,i+1}|}. \quad (4)$$

Here, f_a represents the strength of the active force, $\boldsymbol{r}_{i-1,i+1} = \boldsymbol{r}_{i-1} - \boldsymbol{r}_{i+1}$ is the vector between the position of the monomers $i-1$ and $i + 1$. According to Eq. (4), the tethered polymer chain will be stretched when $f_a < 0$, and it will be compressed when $f_a > 0$. It was found that semiflexible polymers under compression often show complex conformational and dynamical behaviors [32–35,41,42]. Motivated by this,

we here only consider the case $f_a \geqslant 0$, and study the conformational and dynamical properties of the polymer under the compression of the active force.

The motion of each monomer from 2 to N is described by the Langevin equation:

$$m\frac{d\boldsymbol{v}}{dt} = -\nabla(U_{LJ} + U_{\mathrm{FENE}} + U_{\mathrm{bend}}) + \boldsymbol{F}_a - \eta v + \boldsymbol{F}^T \quad (5)$$

Here m is the mass of the monomer, η is the friction coefficient, and $\boldsymbol{F}^{\mathrm{T}}$ is the random force with $\langle \boldsymbol{F}^T(t) \rangle = 0$ and $\langle \boldsymbol{F}^T(t) \cdot \boldsymbol{F}^T(t') \rangle = 6\eta k_B T \delta(t - t')$, where k_B is the Boltzmann constant and T is the temperature. To calculate Eq. (5), we adopt the velocity Verlet algorithm with a time step $\Delta t = 0.005$.

At the beginning of the simulation, the polymer is generated above the surface with the head monomer fixed at $(0, 0, \sigma)$. We first set $f_a = 0$ and run a long time ($\geqslant 10^6$ steps) of Brownian motion to equilibrate the polymer. We then switch on the active force and run a long steady time ($> 1.5t_b$; t_b is the buckling time which will be defined in Sec. III B) to let the polymer reach the final steady state where the average properties do not change obviously with time. After that, we continue run a long sampling time ($= 10^6$ time steps), in which the conformational and the dynamical properties of the polymer at the steady state are sampled and studied. All the statistical results in our work are averaged over 1000 independent runs. In each independent run, 20 samples are collected at intervals of 5×10^4 time steps. Therefore, the statistical quantities of the tethered active polymer chains are averaged over 20 000 samples, and the errors of ensemble averages are very small.

In this work, σ, m, and $k_B T$ are chosen as the units of length, mass, and energy, respectively. So, the time scale and the force scale are given by $t_{LJ} = (m\sigma^2/k_B T)^{1/2}$ and $f_0 = k_B T/\sigma$, respectively. In the simulation, we choose $\varepsilon_0 = 1$, $k = 15$, and $R_0 = 2$, and set $\eta = 10$ to ensure the overdamped motion of monomers [40]. Moreover, the polymer length is taken to be $N = 100$, unless explicitly mentioned. We mainly study the influence of f_a and k_b on the conformational and dynamical properties of the polymer chain.

III. SIMULATION RESULTS AND DISCUSSION

A. Steady properties

Since the interaction between the polymer and the surface is purely repulsive, the polymer is stretched along the z direction at $f_a = 0$, while when $f_a > 0$, monomers tend to move towards the fixed monomer under the propulsion of the tangential active force. Figure 2 shows the dependence of the steady end-to-end distance, R_{es}, on f_a for different k_b, where $N = 100$. When f_a is small, R_{es} is nearly independent of f_a, meaning that the influence of the active force on the polymer is negligible. When f_a is moderate, R_{es} decreases quickly with increasing f_a, indicating that the polymer is compressed. The compression could cause the bend of the polymer. For a given f_a, the larger k_b is the weaker the compression is, leading to the monotonic increase of R_{es} with increasing k_b, while when f_a is very large ($f_a > 10$), the size of the polymer is very small, and the excluded volume interaction between monomers will prevent the polymer from being compressed
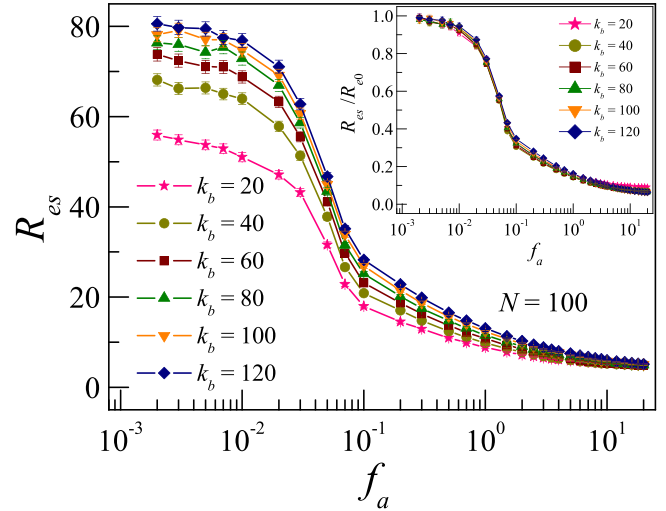
FIG. 2. The dependence of the steady end-to-end distance R_{es} on f_a for different k_b, where $N = 100$. The inset shows the dependence of the ratio R_{es}/R_{e0} on f_a for different k_b, where $N = 100$, and R_{e0} represents the value of R_{es} at $f_a = 0$.

further, resulting in R_{es} tending to be the same constant value for different k_b, as shown in Fig. 2. The inset of Fig. 2 shows the dependence of the ratio R_{es}/R_{e0} on f_a for different k_b, where R_{e0} represents the value of R_{es} at $f_a = 0$. At the small or moderate f_a region, it is interesting to see that all the curves overlap with each other on a main curve, meaning that the dependence of R_{es}/R_{e0} on f_a is independent of k_b.

It was found that the semiflexible polymer chain may form helical or spiral conformation under the compression of the spatial confinement or self-propelled active force [22,27,41]. In our work, the structure of the polymer at the steady state is determined by the competition between the external active force and the bending energy. When f_a is very small, the bending energy dominates, then the polymer often adopts extended conformation and is nearly undisturbed by the active force. While when f_a is moderate, the active force becomes comparable to the bending energy, causing a remarkable compression of the polymer. To examine the conformational property of the polymer chain under the compression of the active force, we have studied the tangent-tangent correlation function $C(i)$ [27], which is defined as

$$C(i) = \frac{\boldsymbol{r}_{1,3}}{|\boldsymbol{r}_{1,3}|} \cdot \frac{\boldsymbol{r}_{i-1,i+1}}{|\boldsymbol{r}_{i-1,i+1}|} \quad (1 < i < N), \quad (6)$$

where $\frac{\boldsymbol{r}_{1,3}}{|\boldsymbol{r}_{1,3}|}$ and $\frac{\boldsymbol{r}_{i-1,i+1}}{|\boldsymbol{r}_{i-1,i+1}|}$ represent the unit tangent vectors at monomers 2 and i, respectively.

Figure 3 shows the dependence of $C(i)$ on i for different f_a and k_b. For small f_a [e.g., $f_a = 0.01$ and 0.1 in Fig. 3(a)] or small k_b [e.g., $k_b = 10$ and 20 in Fig. 3(b)], $C(i)$ decays exponentially or shows remarkable damping oscillation, indicating that the correlation between tangent vectors at the second and the ith monomer is weaker and weaker with increasing i, while for large f_a and large k_b, $C(i)$ shows periodical oscillation with nearly constant amplitude, meaning that the correlation between tangent vectors is strong and long range, which is similar to that of the helical conformation structure [41].
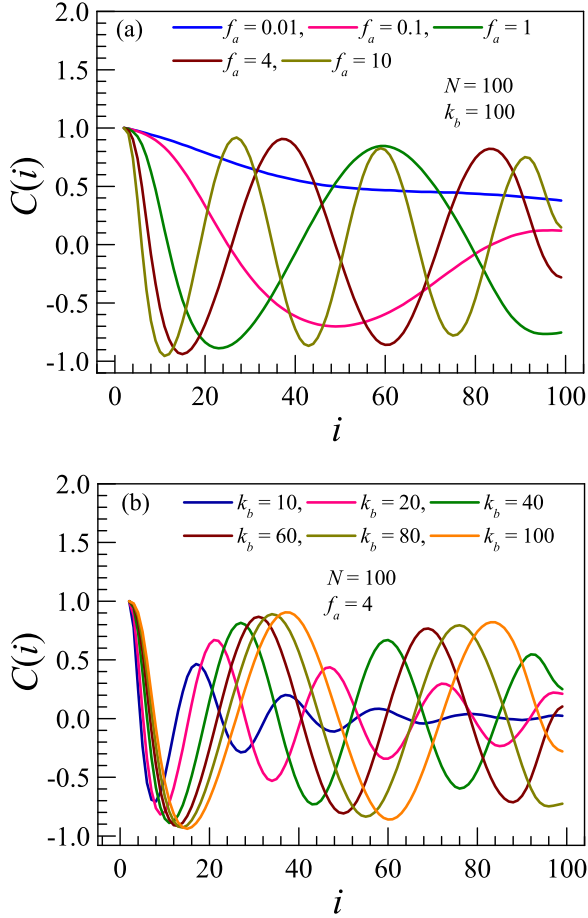
FIG. 3. The tangent-tangent correlation function $C(i)$ for (a) different f_a at $N = 100$ and $k_b = 100$, (b) different k_b at $N = 100$ and $f_a = 4$.

In the following, we will focus on the polymer properties in the parameter region with $f_a \geqslant 1$ and $k_b \geqslant 40$, where the polymer is compressed by the active force and the correlations between tangent vectors are strong. We have specially examined the configuration of the polymer chain at large f_a and large k_b, and found that the polymer is often buckled into a quasihelical structure. The typical snapshot of the quasihelical structure is shown in Fig. 4 for $N = 100$, $k_b = 100$, and
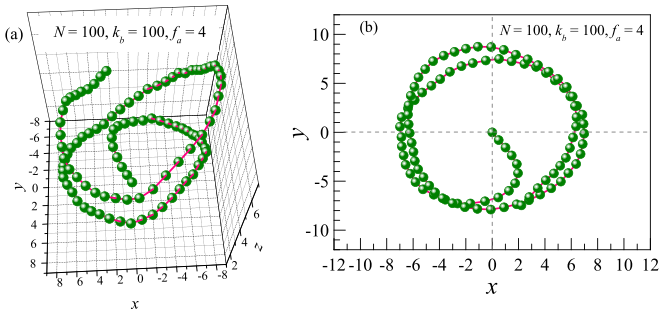
FIG. 4. The typical snapshot of the quasihelical structure of the polymer chain at the steady state, where $N = 100$, $k_b = 100$, and $f_a = 4$. (a) the positions of monomers in 3D space, (b) the projections of monomers on the xoy plane.
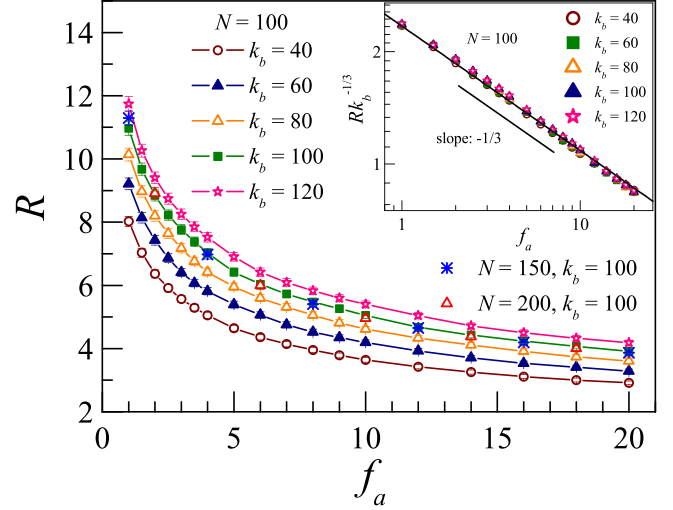
FIG. 5. The dependence of radius of the quasihelical structure, R, on f_a for different k_b and N. The inset shows the dependence of the product $Rk_b^{-1/3}$ on f_a for different k_b, where $N = 100$.

$f_a = 4$. We can see that the polymer chain winds around the z axis, and the projections of monomers on the xoy plane distribute nearly symmetrically around the origin of coordinate (the head monomer).

It is well known that passive semiflexible polymers confined in the nanochannel can also form helical configurations under a compressive axial force. In fact, the compression deformations are dependent on the degree of confinement. For strong confinement (small radius of the nanochannel), the polymer shows complex structural phases upon longitudinal compression force: random deflection along the channel at small force, a helix going around the channel wall at moderate force, and folded structures (double-folded random deflection, double-folded helix, or three-folded structures) at large force [43,44], while for weak confinement (large radius of the nanochannel), a relatively small compressive force can fold the polymer, and then it is difficult for the polymer to form a helical structure [44]. However, in our model, the tangential active force can drive the polymer to form a helical structure without nanochannel confinement, and meanwhile the helical structure is still very stable at large active force.

To describe the size of the quasihelical structure of the polymer, we have calculated the average helical radius (R), which is defined as the average distance between monomers and the z axis, i.e., $R = \frac{1}{N} \sum_{i=1}^{N} \sqrt{x_i^2 + y_i^2}$, where x_i and y_i are the x and y coordinates of the ith monomer, respectively. Figure 5 shows the dependence of R on f_a and N for different k_b. With an increase in f_a, R decreases monotonically, consistent with the dependence of the steady end-to-end distance R_{es} on f_a as shown in Fig. 2. R is also dependent on k_b. R increases monotonically with increasing k_b, meaning that it is more and more difficult to bend a stiffer polymer.

According to the theoretical model of Bourdieu *et al.* [37], at the steady state, the bending moment $M \propto k_b/R$ is balanced by the torque $\Gamma \propto fR^2$ produced by the active force. Here, f represents the active force per unit length, which can be roughly expressed as $f = f_a/b_0$ with $b_0 \sim 1.03$ the average
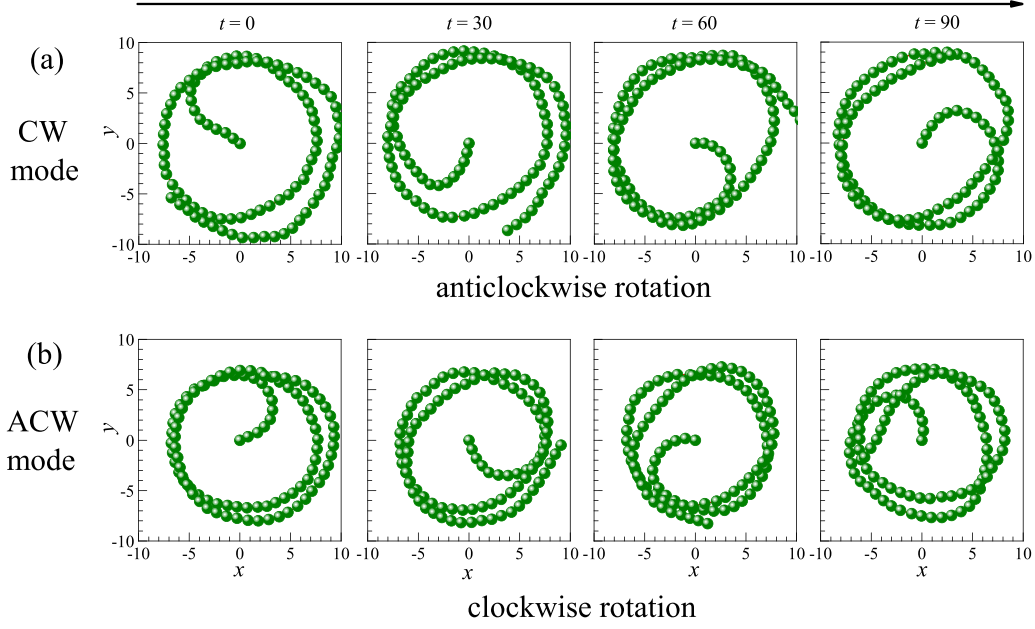
FIG. 6. Time series of the projection of the polymer chain on the xoy plane, where $N = 100$, $k_b = 100$, and $f_a = 4$. (a) Polymer with CW mode undergoes anticlockwise rotation. (b) Polymer with ACW mode undergoes clockwise rotation.

bond length in our model. So, we can obtain from $M = \Gamma$ that

$$R \propto f_a^{-1/3} k_b^{1/3}, \qquad (7)$$

which is in good agreement with our simulation results, as shown in the inset of Fig. 5. This scaling relation is the same as that of the spiral structure of active polymer in 2D space [37]. Moreover, we find that R is nearly independent of N, as shown in Fig. 5. For the quasihelical structure, the polymer spirals upward and around the z axis, and then the increase of the polymer length can increase the length of the helix but not affect the radius of the helix.

Under the driven of the active torque Γ, the whole polymer rotates around the z axis. The rotation direction is dependent on the winding mode of the polymer round the z axis. Viewed against the direction of the z axis, the quasihelical structure has two different winding manners, the clockwise winding mode (CW mode) and the anticlockwise winding mode (ACW mode). For the CW mode, the polymer rotates anticlockwise, while for the ACW mode, the polymer rotates clockwise, as shown in Fig. 6. For each independent simulation, the winding mode of the quasihelical structure is formed randomly, and the emergence probability of each mode is about 50%. Meanwhile, due to the large bond bending rigidity, it is difficult for the polymer to change the winding mode as well as the rotation direction during the rotation process.

We have studied the angular velocity (ω) of the polymer rotation. At large k_b, the polymer chain behaves nearly as a rigid body, and the monomers move nearly uniformly. Therefore, we defined ω as

$$\omega = |L_z|/J = \left| \sum_{i=1}^{N} (x_i v_{iy} - y_i v_{ix}) \right| \bigg/ \sum_{i=1}^{N} (x_i^2 + y_i^2), \qquad (8)$$

where $L_z = \sum_{i=1}^{N} L_{iz} = \sum_{i=1}^{N} m(x_i v_{iy} - y_i v_{ix})$ represents the z component of the polymer's angular momentum, $J =$

$m \sum_{i=1}^{N} (x_i^2 + y_i^2)$ represents the rotational inertia of the polymer with respect to the z axis, $m = 1$ is the mass of the monomer, x_i and y_i are the x and y coordinates of the ith monomer, and v_{ix} and v_{iy} are the x and y components of the velocity of the ith monomer, respectively. Figure 7 shows the dependence of ω on f_a for different N and k_b. We find that ω increases with increasing f_a but decreases with increasing k_b. However, ω is roughly independent of N.

In the overdamped limit, the active force f_a on each monomer is balanced by the frictional force $\eta \omega R$ [37], i.e., $f_a = \eta \omega R$, then we have

$$\omega = f_a/(\eta R)r \qquad (9)$$
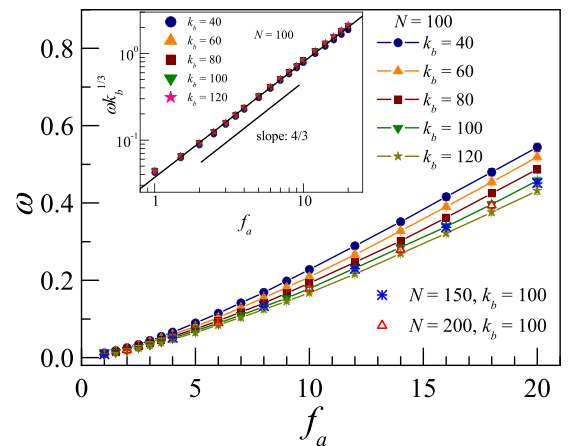
FIG. 7. The dependence of the angular velocity ω on f_a for different N and k_b. The inset shows the dependence of the product $\omega k_b^{1/3}$ on f_a for different k_b, where $N = 100$.
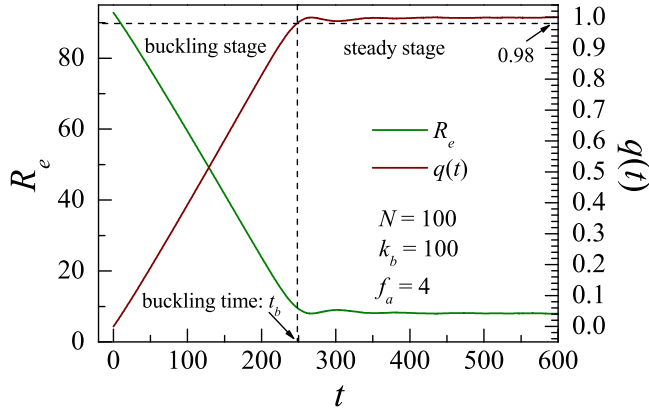
FIG. 8. The evolution of the end-to-end distance R_e and the relaxation function $q(t)$, where $N = 100$, $k_b = 100$, and $f_a = 4$.

From Eqs. (7) and (9), we can get

$$\omega \propto f_a^{4/3} k_b^{-1/3} \qquad (10)$$

This is in good agreement with our simulation results shown in the inset of Fig. 7.

B. Buckling process

In the above section, we have shown that the polymer chain is buckled into quasihelical structures at the steady state for large f_a and k_b. In this section, we will focus on the dynamics of the polymer chain before reaching the final steady state. In our simulation, the polymer chain is first equilibrated with $f_a = 0$ and then subjected to the tangential active force ($f_a > 0$) at $t = 0$. Then, the polymer undergoes a buckling process during which the polymer is compressed gradually and finally forms quasihelical structures. Figure 8 shows the evolution of the end-to-end distance (R_e) of the polymer. The buckling process is characterized by the quick decrease of R_e when t is small, while when t is large, the polymer is at the steady state and then R_e reaches the steady value R_{es}. To roughly determine the elapsed time of the buckling process, we have calculated the relaxation function $q(t) = \frac{R_e(0)-R_e(t)}{R_e(0)-R_{es}}$, and defined the buckling time t_b at which $q(t) = 0.98$, as shown in Fig. 8. Based on t_b, the evolution of the polymer can be specifically divided into two stages: (1) the buckling stage at $t < t_b$, where the polymer is compressed and then R_e decreases gradually, and (2) the steady stage at $t > t_b$, where R_e reaches the steady value, as shown in Fig. 8.

Figures 9(a) and 9(b) show the dependence of the buckling time t_b on the active force f_a and the polymer length N, respectively. We can see that t_b increases monotonically with decreasing f_a or increasing N. Specially, t_b as a function of N and f_a can be expressed by a scaling relation $t_b \propto N^\alpha f_a^{-\beta}$ with $\alpha = 1$ and $\beta = 1$. Intuitively, the polymer is compressed and bended during the buckling process, and then the buckling time t_b should increase monotonically with increasing the polymer rigidity k_b. However, we find that t_b is roughly independent of k_b for any given f_a, as shown in Fig. 9(a). The mechanism of the buckling process of tethered active polymers is different from that of the adsorption process of passive polymers onto attractive surfaces. A significant dif-
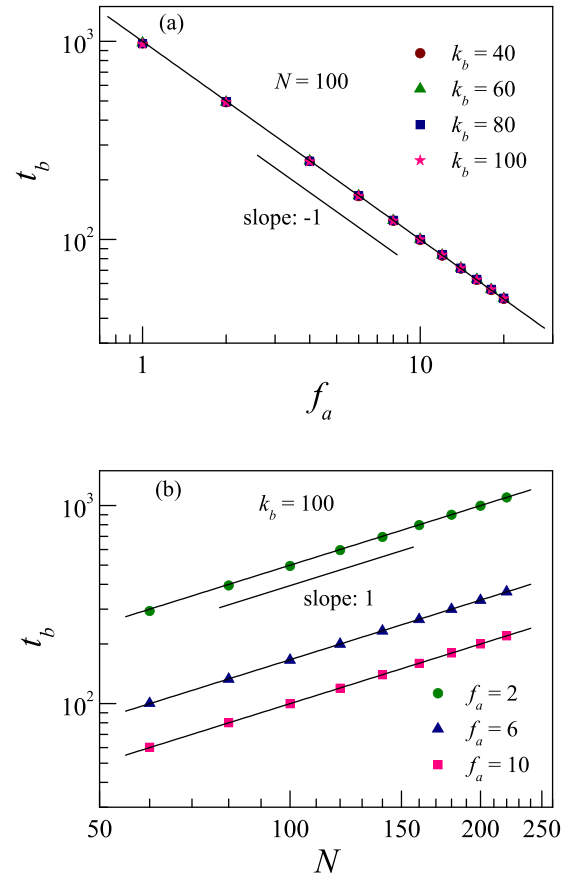
FIG. 9. (a) The dependence of the buckling time t_b on f_a for different k_b, where $N = 100$. (b) The dependence of the buckling time t_b on N for different f_a, where $k_b = 100$. Solid lines are given by Eq. (16).

ference is that the adsorption time τ_{ads} of a passive polymer chain is strongly dependent on the polymer rigidity k_b, i.e., τ_{ads} increases monotonically with increasing k_b [45].

To understand the dependence of t_b on f_a, N, and k_b, we have studied the details of the buckling process. Figure 10 shows a sequence of snapshots of the polymer during the buckling process of a simulation with $N = 100$, $k_b = 100$, and $f_a = 4$, where $t = 0$ represents the time when the active force is just switched on. We can see that the polymer chain at the buckling stage can be roughly divided into two parts, the quasistraight part above the substrate and the quasihelical part near the substrate. As time increases, the length of the quasistraight part decreases, while the length of the quasihelical part increases. We can also see that the quasistraight parts at different times nearly overlap with each other, indicating that the quasistraight part nearly moves along its contour and shows railway motion during the buckling process, which is quite similar to the railway motion of the active polymer in 2D free space or through a narrow pore [22,46]. Accompanied by the railway motion of the quasistraight part, the quasihelical part of the polymer also rotates around the z axis with the increase of its length, as shown in Fig. 10.

The railway motion of the quasistraight part of the polymer during the buckling process can be verified further by the evolution of the mean displacement
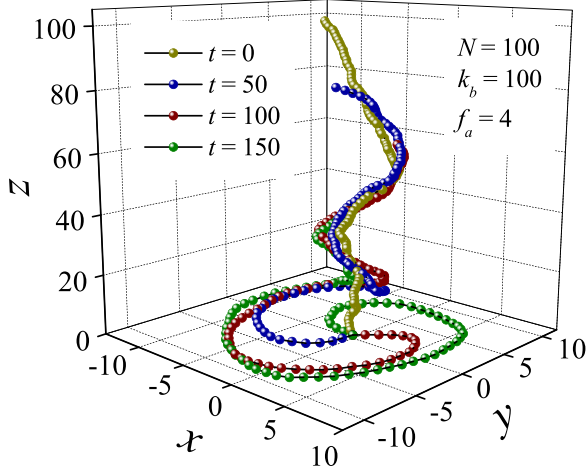
FIG. 10. A sequence of snapshots of the polymer during the buckling process of a simulation, where $N = 100$, $k_b = 100$, and $f_a = 4$.

$\Delta r = \sqrt{(x_{i+j} - x_{i0})^2 + (y_{i+j} - y_{i0})^2 + (z_{i+j} - z_{i0})^2}$ of monomer $i + j$ relative to the position of monomer i at $t = 0$, (x_{i0}, y_{i0}, z_{i0}) [22,46], as shown in Fig. 11, where $N = 100$, $k_b = 100$, $f_a = 4$, and $i = 40$. With t increasing, monomer $i + j$ moves along the contour of the polymer and approaches (x_{i0}, y_{i0}, z_{i0}), resulting that Δr decreases gradually and reaches the minimum value $\Delta r_{\min}$ when monomer $i + j$ is closest to (x_{i0}, y_{i0}, z_{i0}). With t increasing further, monomer $i + j$ leaves (x_{i0}, y_{i0}, z_{i0}), leading to the increase of Δr. When t is large, monomer $i + j$ belongs to the quasihelical part and rotates around the z axis, resulting in Δr showing periodical oscillation. We can see from Fig. 11 that $\Delta r_{\min}$ is very small, meaning that monomer $j + i$ nearly passes through (x_{i0}, y_{i0}, z_{i0}) perfectly during the railway motion. More importantly, we find that Δr varies nearly linearly with t as monomer $i + j$ approaches or leaves (x_{i0}, y_{i0}, z_{i0}), as shown in Fig. 11. Specifically, Δr as a function of t can be expressed as $\Delta r = -v_b t + c_1$ when monomer $i + j$
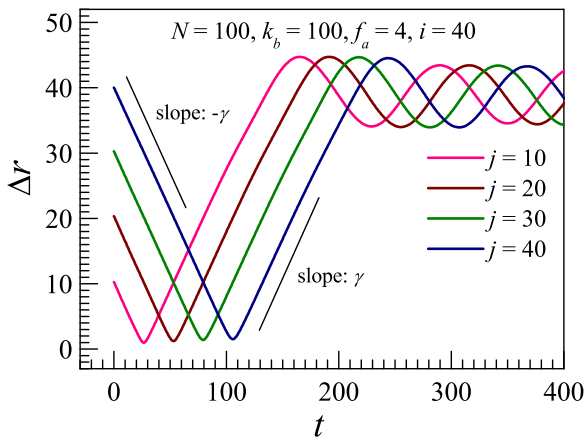
FIG. 11. The evolution of the mean displacement Δr of monomer $i + j$ relative to the position of monomer i at $t = 0$, where $N = 100$, $k_b = 100$, $f_a = 4$, and $i = 40$.
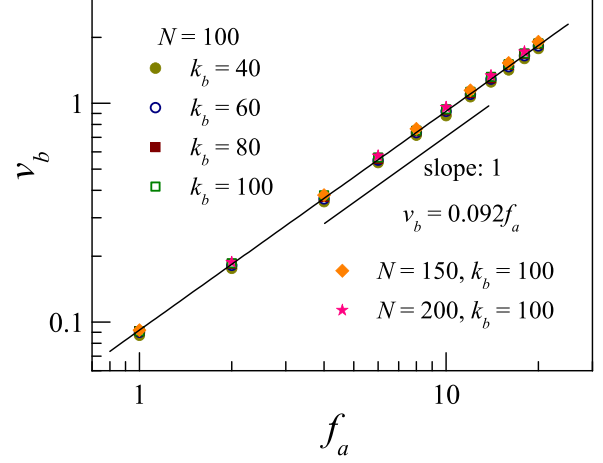
FIG. 12. The dependence of the buckling velocity v_b on f_a for different k_b and N.

approaches (x_{i0}, y_{i0}, z_{i0}), and $\Delta r = v_b t + c_2$ when monomer $i + j$ leaves (x_{i0}, y_{i0}, z_{i0}). The slope v_b is nearly independent of j. This indicates that all the monomers of the quasistraight part of the polymer move along its contour with the same buckling velocity v_b during the buckling process. Figure 12 shows the dependence of the v_b on f_a for different k_b and N. We can see that v_b increases with f_a increasing, but is nearly independent of k_b and N. Specially, v_b as a function of f_a can be described by

$$v_b = 0.092 f_a. \tag{11}$$

During the buckling process, the energy supplied by the active force can be roughly divided into two parts. One part is converted into the bond bend energy, and the other part is dissipated by the viscous force. Since the polymer chain behaves nearly as a rigid body at large k_b, all the monomers of the polymer move nearly synchronously with velocity v, then both the decrement of the length of the quasistraight part and the increment of the length of the quasihelical part of the polymer in a small time interval dt are vdt. So, we have

$$N f_a v dt = N\eta v v dt + \frac{k_b}{2R^2} v dt. \tag{12}$$

Here, the first term is the active energy input into the system, the second term is the energy dissipated by the viscous force, and the third term is the increment of the bond bend energy ($\frac{k_b}{2R^2}$ represents the bond bend energy stored in a polymer fragment of one unit length, and R is the steady radius of the quasihelical structure). From Eq. (12), we can get

$$v = \frac{f_a}{\eta} - \frac{k_b}{2\eta N R^2}. \tag{13}$$

By using the theoretical result of R [Eq. (7)], Eq. (13) can be written as

$$v = \frac{f_a}{\eta} - \frac{k_b^{1/3} f_a^{2/3}}{2\eta N}. \tag{14}$$

For the parameters chosen in our work, the value of the second term on the right is much smaller than that of the first

term, and then Eq. (14) can be expressed approximately as

$$v \approx \frac{f_a}{\eta}, \tag{15}$$

i.e., the velocity v is proportional to f_a, but is nearly independent of k_b and N. Since $\eta = 10$ in our simulation, we can get from Eq. (16) that $v \approx 0.1 f_a$, which is in good agreement with the simulation result shown in Fig. 12.

Based on the buckling velocity v_b, the buckling time t_b can be roughly calculated by

$$t_b \approx N b_0 / v_b \approx \eta N f_a^{-1} \tag{16}$$

with $b_0 (\sim 1.03)$ the average bond length in our model, which is in good agreement with the simulation results, as shown by the solid lines in Fig. 9.

We would like to note that the pathway of the quasistraight part at the buckling stage might depend on the method of relaxation. In our simulation, the active force is switched on immediately after the polymer reaching the equilibrium state, and the polymer is compressed quickly. This means that the quasistraight part does not have enough time to relax, and then it nearly moves along its own contour under the active force, leading to the railway motion manner. So, if f_a is ramped up very slowly, there is long enough time for the polymer to relax, and then the quasistraight part at different time will not overlap with each other, i.e., the move of the quasistraight part will no longer show railway motion manner.

IV. CONCLUSION

The conformational and dynamical properties of a tethered active polymer chain are studied by using Langevin dynamics. The polymer is modeled by a self-avoiding bead-spring chain with each bead being propelled by a tangential active force

(f_a) along the contour of the chain. The head of the polymer is fixed near an infinite flat substrate at $z = 0$. In our simulation, the polymer is equilibrated first at $f_a = 0$ and then subjected to the active force. Under the drive of the active force, the polymer relaxes and reaches the final steady state gradually. It was found that the steady size of the polymer shows monotonic decrease with f_a increasing, due to the compression of the active force. Specially, when the active force (f_a) and the bending rigidity (k_b) are large, the polymer at steady state forms a quasihelical structure, and rotates around the z axis. Both the radius of the quasihelical structure (R) and the angular velocity of the rotation (ω) are nearly independent of the polymer length (N), but show scaling relations with f_a and k_b, i.e., $R \propto f_a^{-1/3} k_b^{1/3}$ and $\omega \propto f_a^{4/3} k_b^{-1/3}$, which can be well understood by simple dynamical models.

Before reaching the steady state, the polymer undergoes a buckling process, during which the polymer is compressed and buckled into a quasihelical structure gradually by the active force. At the buckling stage, the polymer can be roughly divided into a quasistraight part above the substrate and a quasihelical part near the substrate. During the buckling process, the length of the quasistraight part decreases, while the length of the quasihelical part increases gradually. Interestingly, the quasistraight part moves in a railway-motion manner with a constant buckling velocity (v_b). It was found that v_b is only proportional to the active force f_a, resulting that the buckling time (t_b) is nearly independent of k_b but shows a simple scaling relation with f_a and N, i.e., $t_b \propto N f_a^{-1}$.

[1] S. J. Kron and J. A. Spudich, Fluorescent actin filaments move on myosin fixed to a glass surface, Proc. Natl. Acad. Sci. USA **83**, 6272 (1986).

[2] J. Borejdo and S. Burlacu, Velocity of movement of actin filaments in in vitro motility assay: Measured by fluorescence correlation spectroscopy, Biophys. J. **61**, 1267 (1992).

[3] L. Liu, E. Tüzel, and J. L. Ross, Loop formation of microtubules during gliding at high density, J. Phys.: Condens. Matter **23**, 374104 (2011).

[4] A. Maloney, L. J. Herskowitz, and S. J. Koch, Effects of surface passivation on gliding motility assays, PLoS One **6**, e19522 (2011).

[5] H. Palacci, O. Idan, M. J. Armstrong, A. Agarwal, T. Nitta, and H. Hess, Velocity fluctuations in kinesin-1 gliding motility assays originate in motor attachment geometry variations, Langmuir **32**, 7943 (2016).

[6] A. Lam, C. Curschellas, D. Krovvidi, and H. Hess, Controlling self-assembly of microtubule spools via kinesin motor density, Soft Matter **10**, 8731 (2014).

[7] D. Nishiguchi, J. Iwasawa, H. R. Jiang, and M. Sano, Flagellar dynamics of chains of active janus particles fueled by an ac electric field, New J. Phys. **20**, 015002 (2018).

[8] Y. Sasaki, Y. Takikawa, V. S. R. Jampani, H. Hoshikawa, T. Seto, C. Bahr, S. Herminghaus, Y. Hidaka, and H. Orihara, Colloidal caterpillars for cargo transportation, Soft Matter **10**, 8813 (2014).

[9] B. Alberts, A. Johnson, J. Lewis, M. Raff, K. Roberts, and P. Walter, *Molecular Biology of the Cell* (Garland Science, Oxford, 2007).

[10] A. S. Bhadwal, N. J. Mottram, A. Saxena, I. C. Sage, and C. V. Brown, Electrically controlled topological micro cargo transportation, Soft Matter **12**, 2961 (2020).

[11] A. F. Demirörs, M. T. Akan, E. Poloni, and A. R. Studart, Active cargo transport with janus colloidal shuttles using electric and magnetic fields, Soft Matter **14**, 4741 (2018).

[12] J. Elgeti, R. G. Winkler, and G. Gompper, Physics of microswimmers-single particle motion and collective behavior: a review, Rep. Prog. Phys. **78**, 056601 (2015).

[13] A. Ghosh and N. S. Gov, Dynamics of active semiflexible polymers, Biophys. J. **107**, 1065 (2014).

[14] D. Osmanović and Y. Rabin, Dynamics of active rouse chains, Soft Matter **13**, 963 (2017).

[15] S. K. Anand and S. P. Singh, Conformation and dynamics of a self-avoiding active flexible polymer, Phys. Rev. E **101**, 030501(R) (2020).

[16] T. Eisenstecken, G. Gompper, and R. G. Winkler, Conformational properties of active semiflexible polymers, Polymers **8**, 304 (2016).

[17] N. Samanta and R. Chakrabarti, Chain reconfiguration in active noise, J. Phys. A: Math. Theor. **49**, 195601 (2016).

[18] T. Eisenstecken, G. Gompper, and R. G. Winkler, Internal dynamics of semiflexible polymers with active noise, J. Chem. Phys. **146**, 154903 (2017).

[19] A. Martín-Gómez, G. Gompper, and R. Winkler, Active brownian filamentous polymers under shear flow, Polymers **10**, 837 (2018).

[20] J. Shin, A. G. Cherstvy, W. K. Kim, and R. Metzler, Self-subdiffusion in solutions of star-shaped crowders: Non-monotonic effects of inter-particle interactions, New J. Phys. **17**, 113028 (2015).

[21] A. Martín-Gómez, T. Eisenstecken, G. Gompper, and R. G. Winkler, Active brownian filaments with hydrodynamic interactions: Conformations and dynamics, Soft Matter **15**, 3957 (2019).

[22] R. E. Isele-Holder, J. Elgeti, and G. Gompper, Self-propelled worm-like filaments: Spontaneous spiral formation, structure, and dynamics, Soft Matter **11**, 7181 (2015).

[23] R. E. Isele-Holder, J. Jäger, G. Saggiorato, J. Elgeti, and G. Gompper, Dynamics of self-propelled filaments pushing aload, Soft Matter **12**, 8495 (2016).

[24] A. K. Manna, P. B. S. Kumar, and R. Adhikari, Colloidal transport by active filaments, J. Chem. Phys. **146**, 024901 (2017).

[25] V. Bianco, E. Locatelli, and P. Malgaretti, Globulelike Conformation and Enhanced Diffusion of Active Polymers, Phys. Rev. Lett. **121**, 217802 (2018).

[26] E. Locatelli, V. Bianco, and P. Malgaretti, Activity-induced Collapse and Arrest of Active Polymer Rings, Phys. Rev. Lett. **126**, 097801 (2021).

[27] S. K. Anand and S. P. Singh, Structure and dynamics of a self-propelled semiflexible filament, Phys. Rev. E **98**, 042501 (2018).

[28] H. J. Jiang and Z. H. Hou, Motion transition of active filaments: rotation without hydrodynamic interactions, Soft Matter **10**, 1012 (2014).

[29] M. S. E. Peterson, M. F. Hagan, and A. Baskaran, Statistical properties of a tangentially driven active filament, J. Stat. Mech. (2020) 013216.

[30] Y. Man and E. Kanso, Morphological transitions of axially-driven microfilaments, Soft Matter **15**, 5163 (2019).

[31] G. D. Canio, E. Lauga, and R. E. Goldstein, Spontaneous oscillations of elastic filaments induced by molecular motors, J. R. Soc. Interface **14**, 20170491 (2017).

[32] F. Ling, H. Guo, and E. Kanso, Instability-driven oscillations of elastic microfilaments, J. R. Soc. Interface **15**, 20180594 (2018).

[33] A. Vilfan, S. Subramani, E. Bodenschatz, R. Golestanian, and I. Guido, Flagella-like beating of a single microtubule, Nano Lett. **19**, 3359 (2019).

[34] R. Chelakkot, A. Gopinath, L. Mahadevan, and M. F. Hagan, Flagellar dynamics of a connected chain of active, polar, brownian particles, J. R. Soc. Interface **11**, 20130884 (2014).

[35] Y. Fily, P. Subramanian, T. M. Schneider, R. Chelakkot, and A. Gopinath, Buckling instabilities and spatio-temporal dynamics of active elastic filaments, J. R. Soc. Interface **17**, 20190794 (2020).

[36] K. Sekimoto, N. Mori, K. Tawada, and Y. Y. Toyoshima, Symmetry Breaking Instabihties of an in Vitro Biological System, Phys. Rev. Lett. **75**, 172 (1995).

[37] L. Bourdieu, T. Duke, M. B. Elowitz, D. A. Winkelmann, S. Leibler, and A. Libchabe, Spiral Defects in Motility Assays: A Measure of Motor Protein Force, Phys. Rev. Lett. **75**, 176 (1995).

[38] A. Laskar, R. Singh, S. Ghose, G. Jayaraman, P. B. S. Kumar, and R. Adhikari, Hydrodynamic instabilities provide a generic route to spontaneous biomimetic oscillations in hemomechanically active filaments, Sci. Rep. **3**, 1964 (2013).

[39] G. H. Xu, F. G. Li, J. C. Wu, and B. Q. Ai, Rectification of an active polymer chain with chirality in a transversal asymmetric channel, Phys. A (Amsterdam, Neth.) **575**, 126051 (2021).

[40] C. Shen, C. R. Qin, T. L. Xu, K. Chen, and W. D. Tian, Structure and dynamics of an active polymer adsorbed on the surface of a cylinder, Soft Matter **18**, 1489 (2022).

[41] Z. Y. Yang, D. Zhang, L. X. Zhang, H. P. Chen, Ateeq-ur-Rehman, and H. J. Liang, Local coil-helix transition of semiflexible polymers confined in spheres, Soft Matter **7**, 6836 (2011).

[42] R. Chelakkot, R. G. Winkler, and G. Gompper, Flow-induced Helical Coiling of Semiflexible Polymers in Structured Microchannels, Phys. Rev. Lett. **109**, 178101 (2012).

[43] Y. Hayase, T. Sakaue, and H. Nakanishi, Compressive response and helix formation of a semiflexible polymer confined in a nanochannel, Phys. Rev. E **95**, 052502 (2017).

[44] W. Chen, X. Kong, Q. Wei, H. Chen, J. Liu, and D. Jiang, Compression and stretching of confined linear and ring polymers by applying force, Polymers **13**, 4193 (2021).

[45] X. Yang, Q. H. Yang, Y. Fu, F. Wu, J. H. Huang, and M. B. Luo, Study on the adsorption process of a semi-flexible polymer onto homogeneous attractive surfaces, Polymer **172**, 83 (2019).

[46] C. Wang, H.-X. Hu, Y.-L. Zhou, B. Zhao, and M.-B. Luo, Translocation of a self-propelled polymer through a narrow pore, Chin. J. Polym. Sci. (2022), doi: 10.1007/s10118-022-2768-3.